Charge-Insensitive Single-Atom Spin-Orbit Qubit in Silicon

Joe Salfi, Jan A. Mol, Dimitrie Culcer, and Sven Rogge

Phys. Rev. Lett. **116**, 246801 — Published 14 June 2016

DOI: 10.1103/PhysRevLett.116.246801

A charge-insensitive single-atom spin-orbit qubit in silicon

Joe Salfi,[1,2] Jan A. Mol,[1,2] Dimitrie Culcer,[1] and Sven Rogge[1,2]

[1] *School of Physics, The University of New South Wales, Sydney, NSW 2052, Australia.*

[2] *Centre for Quantum Computation and Communication Technology, The University of New South Wales, Sydney, NSW 2052, Australia.*

(Dated: May 23, 2016)

Abstract

High fidelity entanglement of an on-chip array of spin qubits poses many challenges. Spin-orbit coupling (SOC) can ease some of these challenges by enabling long-ranged entanglement via electric dipole-dipole interactions, microwave photons, or phonons. However, SOC exposes conventional spin qubits to decoherence from electrical noise. Here we propose an acceptor-based spin-orbit qubit in silicon offering long-range entanglement at a sweet spot where the qubit is protected from electrical noise. The qubit relies on quadrupolar SOC with the interface and gate potentials. As required for surface codes, 10^5 electrically mediated single-qubit and 10^4 dipole-dipole mediated two-qubit gates are possible in the predicted spin lifetime. Moreover, circuit quantum electrodynamics with single spins is feasible, including dispersive readout, cavity-mediated entanglement, and spin-photon entanglement. An industrially relevant silicon-based platform is employed.

PACS numbers: 71.70.Ej,73.21.La,42.50.Pq,03.67.-a,03.67.Lx

In recent years, the coherence and control fidelity of solid-state qubits has dramatically improved[1–5] and spin qubits[6–8] with highly desirable properties have been demonstrated.[9, 10] However, many obstacles remain to efficiently entangle a large array of spin qubits on a chip. For example, exchange is inherently vulnerable to decoherence from electrical fluctuations[11–13], coupling spin to charge noise. Minimizing decoherence and improving control in the face of noise is the key issue for large-scale quantum computing, because it ultimately determines if the error-correction resources can be managed for a large qubit array.[14] Moreover, exchange-based entanglement is inherently short-ranged, making fabrication challenging for gates in quantum dot arrays[6], and placing strict demands on Si:P donor placement.[7]

Here we propose a single-acceptor spin-orbit qubit where the unique properties of hole spins give a host of desirable attributes. First, spin-orbit coupling (SOC) enables long-ranged entanglement via microwave photons or electric dipole-dipole interactions[15–25], of interest for hybrid quantum systems[26–30], improving error correction[31], and reducing fabrication demands compared with exchange coupled schemes. Second, and most remarkably, we find a sweet spot where coherence is insensitive to electrical noise and electric dipole spin resonance[32–34] (EDSR) is maximized. Consequently, coherence and gate timings are protected from electrical noise at the Hamiltonian level, and one- and two-qubit gate times are optimized. In comparison, electric field noise dephases conventional spin-orbit qubits[35, 36] and acceptor charge qubits.[23, 37] The coherence of our spin-orbit qubit benefits from reduced hyperfine coupling of holes[38] and ^{28}Si enrichment[39], and has much longer phonon relaxation times than acceptor charge qubits.[23, 37] Finally, the acceptors naturally confine single holes that can be manipulated in silicon nanoelectronic devices[40].

The exceptional properties of the qubit derive from the quadrupolar SOC[41–44] contained in the spin-3/2 Luttinger Hamiltonian[45] and in the interaction with the inversion asymmetric interface potential, not studied previously for acceptors. This SOC is unusually strong for acceptors because it acts directly on the low-energy spin manifold, contrasting its indirect role in hole quantum dots.[19, 20, 46–49] The SOC must be considered non-perturbatively to obtain the sweet spot, and the interface strongly enhances EDSR relative to a bulk acceptor. We find 0.2 ns one-qubit gate times, charge-noise immunity, and long phonon relaxation times at the sweet spot, allowing for $> 10^5$ operations in the coherence time. Two-qubit entanglement based on spin-dependent electric dipole-dipole interactions[15–17] is feasible with $\sqrt{\mathrm{SWAP}}$ times of 2 ns, and 10^4 operations in the coherence time. EDSR also enables circuit quantum electrodynamics[26–30] (cQED) with single-spin dispersive readout, and long distance spin-spin entanglement with $\sqrt{\mathrm{SWAP}}$ times of 200 ns. Resonant spin-photon coupling with $g_c = 5$ MHz is also feasible.

Qubit Concept. The qubit is a hole spin bound to a single Si:B dopant[40, 50, 51], implanted[52] or placed by scanning tunneling microscopy[53, 54] near an interface, in a strained silicon-on-insulator (SOI) substrate (Fig. 1A). The key quadrupolar interactions, associated with interface inversion asymmetry and products $\{J_i, J_j\} = (J_iJ_j + J_jJ_i)$ of spin-3/2 matrices where $i(j) = x, y, z$, originate from strong SOC in the valence band, and have no analog in the conduction band.[41–44] This SOC acts on the 4×4 ground state manifold $|\Psi_{m_J}\rangle$, *i.e.*, the $m_J = \pm\frac{3}{2}$ and $m_J = \pm\frac{1}{2}$ Kramers doublets composed mostly of $\left|J = \frac{3}{2}, m_J\right\rangle$ Bloch states.[55] For Si:B they are well isolated by ~ 20 meV from orbital excited states and 46 meV from the valence band edge[56] (Fig. 1B).

The key quadrupolar interactions include the acceptor hole spin-mixing that is linear in electric fields, $H_{\mathrm{E,ion}} = 2p/\sqrt{3}(E_z\{J_x, J_y\} + \mathrm{c.p})$, associated with T_d symmetry in the central cell [57]. Here, $p = 0.26$ D is known for Si:B[58] (1 D = 0.021 e·nm). An electric field E_z further breaks the envelope function parity by mixing excited states outside the $|\Psi_{m_J}\rangle$ manifold.[55] Projected into the $|\Psi_{m_J}\rangle$ subspace, this interaction is governed by $H_E = b(J_z^2 - \frac{5}{4}I)E_z^2 + (2d/\sqrt{3})(\{J_y, J_z\}E_yE_z + \{J_z, J_x\}E_zE_x)$, where b and d split and mix the doublets, respectively. We verified that this holds for triangular interface wells, using (i) a Schrieffer-Wolff transformation[59, 60] with higher excited states in the spherical spin-3/2 basis[61], and (ii) numerical, non-perturbative Luttinger-Kohn (LK) calculations with explicit ion and interface well potentials[62, 63]. We find a splitting $\Delta_W(E_z) = \Delta_{\mathrm{if}} + \Delta_G(E_z)$ (Fig. 1B), where Δ_{if} from the interface is larger for shallower acceptors (in agreement with experiments[50]), and $\Delta_G(E_z) \propto E_z$ increases with increasing field. Moreover, quadrupolar SOC combining inversion asymmetry and in-plane electric fields is governed by terms $\alpha(E_z)E_{x,y} \propto E_zE_{x,y}$ that replace $dE_zE_{x,y}$ in H_E.

Operating point and sweet spot. Here we show that the qubit splitting $\hbar\omega$ (between $|+\rangle$ and $|-\rangle$, Fig. 1B) in an in-plane magnetic field $\hat{\mathbf{y}}B$ depends on the electric field E_z applied by the gates (Fig. 1A), and at the sweet spot, $\hbar\omega$ is insensitive to electric-field noise $\delta\mathbf{E}$ in all directions. Including magnetic fields, strain Δ_ϵ (Supplemental Material[64]) and the

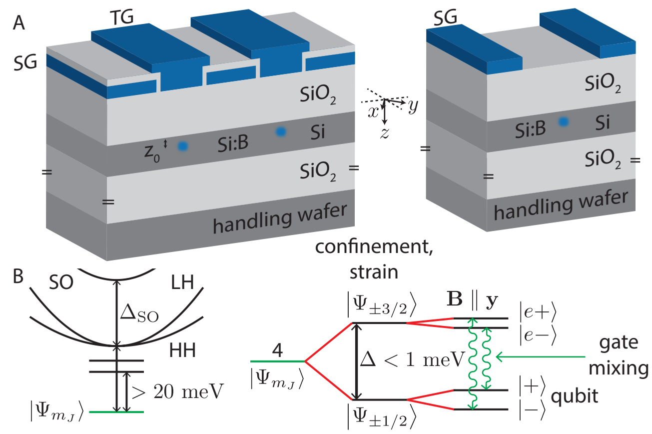

FIG. 1. A. Device schematic, showing near-interface Si:B impurity with gates to SG and TG to apply in-plane and vertical electric fields, respectively (left), or for cQED, gates forming the resonator apply both the in-plane and vertical electric fields (right). An in-plane applied magnetic field ensures a long photon lifetime in the superconductor resonator. B. Electronic structure of an acceptor, where the splitting Δ is determined by the strain, interface, and gate field E_z. Shown: pE_z-induced mixing of states in the 4×4 manifold due to the T_d symmetry in the unit cell of the ion. Not shown: LH-HH coupling from in-plane drive fields.

interface well, but not in-plane electric fields, we find an operating point Hamiltonian,

$$H_{\mathrm{op}} = \begin{pmatrix} \Delta(E_z) & -i\varepsilon_Z & i\frac{\sqrt{3}}{2}\varepsilon_Z & -ipE_z \\ i\varepsilon_Z & \Delta(E_z) & ipE_z & -i\frac{\sqrt{3}}{2}\varepsilon_Z \\ -i\frac{\sqrt{3}}{2}\varepsilon_Z & -ipE_z & 0 & 0 \\ ipE_z & i\frac{\sqrt{3}}{2}\varepsilon_Z & 0 & 0 \end{pmatrix} \tag{1}$$

in the basis $\{|\Psi_{-1/2}\rangle, |\Psi_{1/2}\rangle, |\Psi_{-3/2}\rangle, |\Psi_{3/2}\rangle\}$, where $\varepsilon_Z = g_1\mu_B B$, μ_B is the Bohr magneton, $g_1 = 1.07$ is the Landé g-factor for Si:B.[58], and $\Delta(E_z) = \Delta_W(E_z) - \Delta_\epsilon$ is the splitting between the light and heavy holes. The cubic g-factor[58] $g_2 \ll g_1$ is temporarily neglected.

Inspecting H_{op}, E_z mixes $|\Psi_{\pm 1/2}\rangle$ and $|\Psi_{\mp 3/2}\rangle$ and these states have an avoided crossing when the interface well splitting compensates strain, *i.e.*, $\Delta(E_z^0) = 0$. In Fig. 1A we show that for appropriate strains $\Delta_\epsilon > \Delta_{\mathrm{if}}$, the anti-crossing can be obtained at $E_z^0 \sim 15$ MV/m for $z_0 \sim 5$ nm acceptor depths.

The field E_z^0 at such an anti-crossing is large enough that the level-repulsion gap $\Delta_{\mathrm{gap}} = 2pE_z^0$ exceeds the Zeeman interactions, *i.e.*, $\varepsilon_Z/\Delta_{\mathrm{gap}} \sim 0.1$. This unusual aspect of our hole spin-orbit qubit *c.f.* other proposals[15–20] follows from the tunabil-

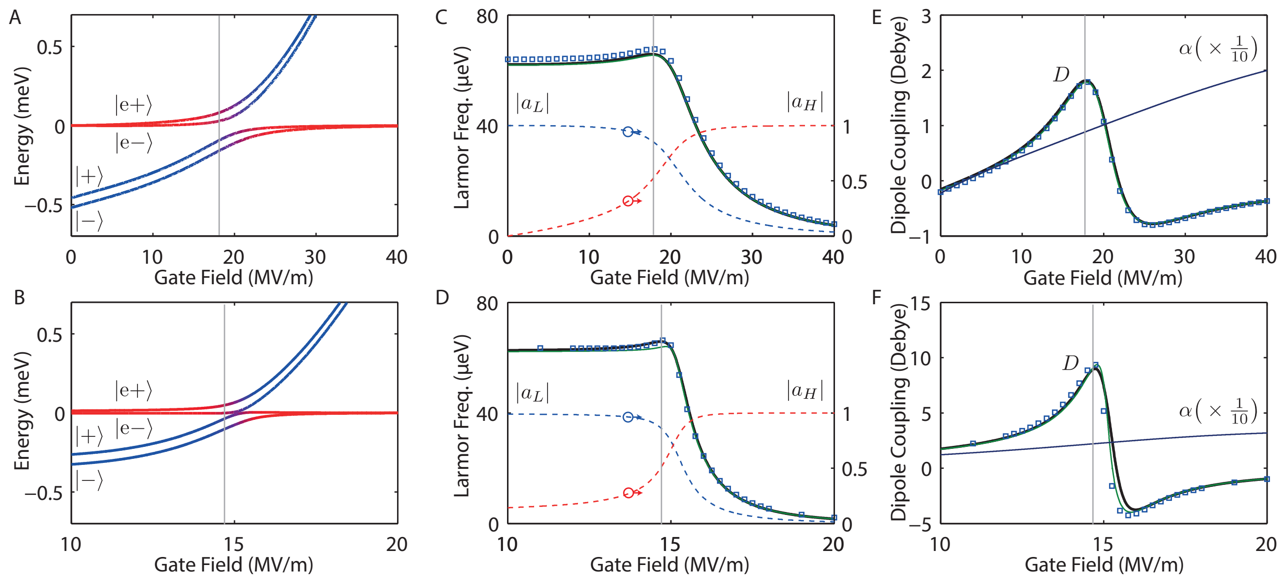

FIG. 2. Spin qubit levels $\varepsilon_\pm$ and $\varepsilon_{u\pm}$ for (A) $z_0 = 4.6$ nm and (B) $z_0 = 6.9$ nm, to zeroth order in $\lambda_{Zo}/(\varepsilon_u - \varepsilon_l)$. Qubit frequency for (C) $z_0 = 4.6$ nm and (D) $z_0 = 6.9$ nm using approximate (black), analytic (green), and full numerical (blue squares) models, in $B_0 = 0.5$ T. Spectral weights $|a_L|$ (blue dashed) and $|a_H|$ (red dashed) are shown. EDSR coupling D for (E) $z_0 = 4.6$ nm and (F) $z_0 = 6.9$ nm. We take $\Delta_\epsilon = 0.62$ meV (0.34 meV) for $z_0 = 4.6$ nm (6.9 nm) achievable in SOI[65], and exceeding disorder strain[40, 66]. Parameters $\Delta_{\rm if}$, $\Delta_G(E_z)$, and $\alpha(E_z)$ were obtained non-perturbatively in a 6×6 LK basis including the cubic LK terms and the split-off holes.

ity of the spin-3/2 levels with strain and confinement, giving rise to the anti-crossing, and the strength of quadrupolar SOC[58] relative to typical spin qubit Larmor frequencies. We treat the quadrupolar SOC term pE_z by a rotation that maps pE_z exactly to the diagonal, to a basis $\{|l-\rangle, |l+\rangle, |u-\rangle, |u+\rangle\}$ leaving Zeeman terms ε_Z off-diagonal. We obtain $|l\pm\rangle = a_L\left|\Psi_{\pm 1/2}\right\rangle \pm i a_H \left|\Psi_{\mp 3/2}\right\rangle$, a low-energy Kramers pair (energy $\varepsilon_l = \frac{1}{2}(\Delta - \sqrt{\Delta^2 + 4E_z^2p^2})$), and an excited Kramers pair $|u\pm\rangle = a_L\left|\Psi_{\pm 3/2}\right\rangle \mp i a_H\left|\Psi_{\mp 1/2}\right\rangle$ (energy $\varepsilon_u = \frac{1}{2}(\Delta + \sqrt{\Delta^2 + 4E_z^2p^2})$). Here, $a_L = \varepsilon_l/\sqrt{E_z^2p^2 + \varepsilon_l^2}$ and $a_H = \sqrt{1 - a_L^2} = E_z p/\sqrt{E_z^2p^2+\varepsilon_l^2}$. In the basis $\{|l-\rangle, |l+\rangle, |u-\rangle, |u+\rangle\}$ Eq. 1 becomes

$$\bar{H}_{\rm op} = \begin{pmatrix} \varepsilon_l & \frac{1}{2}\lambda_{Zl}^* & \frac{1}{2}\lambda_{Zo}^* & 0 \\ \frac{1}{2}\lambda_{Zl} & \varepsilon_l & 0 & \frac{1}{2}\lambda_{Zo} \\ \frac{1}{2}\lambda_{Zo} & 0 & \varepsilon_u & \frac{1}{2}\lambda_{Zu}^* \\ 0 & \frac{1}{2}\lambda_{Zo}^* & \frac{1}{2}\lambda_{Zu} & \varepsilon_u \end{pmatrix}. \quad (2)$$

Here, the Zeeman terms λ_{Zi} depend explicitly on E_z due to the gate-induced mixing of

$\left|\Psi_{\pm 1/2}\right\rangle$ and $\left|\Psi_{\mp 3/2}\right\rangle$. We find $\lambda_{Zl} = 2\varepsilon_Z(\sqrt{3}a_L a_H - i a_L^2)$, $\lambda_{Zu} = 2\varepsilon_Z(\sqrt{3}a_L a_H - i a_H^2)$ and $\lambda_{Zo} = 2\varepsilon_Z(-a_H a_L + i\frac{\sqrt{3}}{2}a_L^2 - i\frac{\sqrt{3}}{2}a_H^2)$.

We perform a final rotation that exactly maps λ_{Zl} and λ_{Zu} to the diagonal, leaving λ_{Zo} off-diagonal, defining a basis $\{\left|-\right\rangle, \left|+\right\rangle, \left|e-\right\rangle, \left|e+\right\rangle\}$ (see Supplemental Material[64]). To zeroth order in $\lambda_{Zo}/(\varepsilon_u - \varepsilon_l)$, the splitting of the Kramers pair qubit states $\left|+\right\rangle$ and $\left|-\right\rangle$ is $\hbar\omega \approx |\lambda_{Zl}|$. When mixed by the gate electric field, the spin 1/2 and spin 3/2 states with different Zeeman terms define a qubit $\left|\pm\right\rangle$ where $\hbar\omega$ is maximized (independent of electric fluctuations) $\mathbf{z}\delta E_z$ to first order when $\left|l\pm\right\rangle = \frac{\sqrt{3}}{2}\left|\Psi_{\pm 1/2}\right\rangle \pm i(-\frac{1}{2})\left|\Psi_{\mp 3/2}\right\rangle$ (see Supplemental Material[64]). As we will subsequently show, the qubit is also insensitive to in-plane electric noise $\delta E_{x,y}$, while a similar analysis yields another sweet spot at $E_z = 0$.

Energy levels $\varepsilon_\pm = \varepsilon_l \pm \frac{1}{2}|\lambda_{Zl}|$ for the qubit are shown alongside excited levels $\varepsilon_{e\pm} = \varepsilon_u \pm \frac{1}{2}|\lambda_{Zu}|$ for $z_0 = 4.6$ nm (6.9 nm) in Fig. 2A (Fig. 2B). Here, blue (red) hue denotes the amplitude of a_L (a_H). The qubit frequency is shown in Fig. 2C and Fig. 2D for approximate (black) and exact (green) solutions to $H_{\rm op}$, alongside the numerics (squares). The maxima in $\hbar\omega$ in Fig. 2C (Fig. 2D) defines the sweet spot at $E_z = 17$ MV/m (14.8 MV/m), for $|a_L|^2 = 3/4$, as expected. We note that the approximate solution (Fig. 2C,D, black lines) captures the essential behaviour of the analytic model (Fig. 2C,D, green lines). Corrections to Zeeman interactions from interface inversion asymmetry and cubic Landé g-factor, although included in the numerics (squares), have been neglected in the analytic model (green). Note that the interface prevents ionization; although $E_z \sim 15$ MV/m is much smaller than silicon's breakdown field, it well exceeds the ionization field of Si:B.[67]

In-plane electric fields: EDSR and noise immunity. We express interactions with in-plane electric fields in the basis $\{\left|-\right\rangle, \left|+\right\rangle, \left|e-\right\rangle, \left|e+\right\rangle\}$, yielding

$$\tilde{H} = \begin{pmatrix} \varepsilon_l - \frac{\hbar\omega}{2} & 0 & \alpha E_1 + \lambda_{Z_1} & \alpha E_2 + \lambda_{Z_2} \\ 0 & \varepsilon_l + \frac{\hbar\omega}{2} & \alpha E_2 + \lambda_{Z_2} & \alpha E_1 + \lambda_{Z_1} \\ \alpha E_1^* + \lambda_{Z_1}^* & \alpha E_2^* + \lambda_{Z_2}^* & \varepsilon_u - \frac{|\lambda_{Zu}|}{2} & 0 \\ \alpha E_2^* + \lambda_{Z_2}^* & \alpha E_1^* + \lambda_{Z_1}^* & 0 & \varepsilon_u + \frac{|\lambda_{Zu}|}{2} \end{pmatrix}. \tag{3}$$

Here, $\left|+\right\rangle$ and $\left|-\right\rangle$ are our Kramers pair qubit states, $\lambda_{Z_1} \propto \lambda_{Zo}$ and $\lambda_{Z_2} \propto \lambda_{Zo}$ are Zeeman terms, and $E_{1,2}$ are interaction terms with in-plane electric fields, where $E_1 = i(\sin\theta + \eta\cos\theta)E_x + i(\cos\theta + \eta\sin\theta)E_y$, $E_2 = (-\cos\theta + \eta\sin\theta)E_x + (\sin\theta - \eta\cos\theta)E_y$, $\theta = \theta_u - \theta_l$, $\lambda_{Zi} = |E_{Zi}|\exp(i\theta_i)$, and $\eta = p/\alpha$.

The qubit Hamiltonian $H_{\rm qbt} = \hbar\omega\sigma_z + DE_{\parallel}\sigma_x$, where $\hbar\omega$ is the qubit frequency (Fig. 2C,D) and D is the EDSR matrix element (Fig. 2E,F), is obtained by projecting the off-diagonal elements of $\tilde{H}$ to first order in $E_{x,y}$ using a Schrieffer-Wolff transformation.[59, 60] Notably, qubit coherence is protected from in-plane electric noise since $\hbar\omega$ contains no terms to first order in $E_{x,y}$. EDSR drive comes from the transverse coupling $DE_{\parallel}\sigma_x$ in $H_{\rm qbt}$. We obtain $D = \alpha|\lambda_{Zo}|(\varepsilon_l - \varepsilon_u)^{-1}(\alpha\cos(\theta_o - \theta_{\parallel}) + p\sin(\theta_o - \theta_{\parallel}))$, where $\mathbf{E}_{\parallel} = E_{\parallel}(\hat{\mathbf{x}}\cos\theta_{\parallel} + \hat{\mathbf{y}}\sin\theta_{\parallel})$. Interestingly, the small splitting $\varepsilon_u - \varepsilon_l$ essential for spin mixing at the sweet spot also causes strong EDSR, since $D \propto (\varepsilon_u - \varepsilon_l)^{-1}$. Note that the EDSR term is dominated by the inversion asymmetry quadrupolar SOC parameter $\alpha \approx 25$ D (Fig. 2F), since it is $100\times$ larger than the bare T_d SOC parameter p.

Importantly, D can be maximized at the sweet spot by choosing the angle $\mathbf{E}_{\parallel}$ relative to $\mathbf{B}||\hat{\mathbf{y}}$ (see Fig. 2E,F). This yields fast gate times, but it also makes D, and therefore all timings based on EDSR, insensitive to fluctuations in electric field, protecting gate fidelity from noise at the Hamiltonian level. Since $\eta = p/\alpha \sim 0.01$ and $\theta_o = \pi/4$ at the sweet spot, D is maximized with respect to $\theta_{\parallel}$ at $\theta_{\parallel} = -\pi/4 \pm \pi/2$. As shown for $z_0 = 4.6$ nm (6.9 nm) in Fig. 2E (Fig. 2F) D is maximized with respect to E_z for the same choice $\theta_{\parallel}$. This result can be easily obtained analytically, and holds for the analytic (green) and numerical (blue squares) solutions.

Qubit Operation. The one-qubit and two-qubit gates employ EDSR-mediated interactions at the sweet spot, where coherence is protected from noise, and their times τ are minimized and also insensitive to electrical noise. EDSR driven π rotations require $\tau_1 = h/(2DE_{AC}) =$ 1 ns (0.2 ns) for the $z_0 = 4.6$ nm (6.9 nm) deep acceptor, assuming a modest in-plane microwave field $E_{\rm AC} = 500$ V/cm. A $\pi/2$ (0) phase shift realizes a σ_y (σ_x) gate, and σ_z gates can be decomposed into a sequence of σ_x and σ_y gates. Readout can be accomplished by energy-dependent[68] or spin-dependent[69] tunneling, or dispersive readout in cQED.[26] Initialization can be achieved by projective readout followed by spin rotation.

Two-qubit entanglement can be achieved via long-ranged Coulomb interactions, owing to spin-dependent electric dipole-dipole interactions.[15–17] Their strength is given by $J_{dd} = (\mathbf{v}_1\cdot\mathbf{v}_2 R^2 - 3(\mathbf{v}_1\cdot\mathbf{R})(\mathbf{v}_2\cdot\mathbf{R}))/4\pi\epsilon R^5$, where $\mathbf{R}$ is the inter-qubit displacement and $\mathbf{v}_i$ is a spin-dependent charge dipole of qubit i, which has the same magnitude as the EDSR matrix element. For a 20 nm distance with negligible tunnel coupling, we obtain a $\sqrt{\rm SWAP}$ time of $\tau_{2dd} = h/4J_{dd} \approx 2$ ns with $J_{dd} \approx D^2/4\pi\epsilon R^3$. The 10^2 times enhancement of EDSR from the interface reduces τ_{2dd} by 10^4 relative to acceptors in bulk silicon, and 10^5 relative to bare magnetic dipole-dipole coupling. Entanglement by Heisenberg exchange is also possible and exchange is hydrogenic when Δ exceeds J.[51] We note that the advantage that holes do not have valley degrees of freedom[70] which may complicate Heisenberg exchange for electrons in Si.[71]

Circuit QED. Coplanar superconducting microwave cavities could be used to implement cQED including two-qubit gates, dispersive single-spin readout, and strong Jaynes-Cummings coupling on resonance with the cavity.[26, 27, 29] We assume a coplanar waveguide resonator operating at $B = 0.5$ T ($f = 15$ GHz) and a vacuum electric field $E_0 \approx 50$ V/m. This can be obtained using a tapered resonator gap, or a superconducting nanowire resonator.[72] At the sweet spot for $z_0 = 4.6$ nm (6.9 nm), the vacuum Rabi coupling is $g_c = eDE_0 = 2$ neV (10 neV).

For cavity mediated non-demolition readout and qubit coupling, we detune the qubit from the cavity by $\Delta = 4g_c$.[22] Here, the spin state shifts the cavity resonance by $\Delta f = g_c^2/\Delta = 0.25$ MHz (1.25 MHz) for $z_0 = 4.6$ nm (6.9 nm). The two-qubit $\sqrt{\text{SWAP}}$ time is $\tau_{2c} = h/4J_c = 200$ ns for $z_0 = 6.9$ nm, determined by the effective spin-spin interaction[22] $J_c = 2g_c^2/\Delta = 2.5$ MHz. Operating at zero detuning, spin/photon Rabi oscillations require $\hbar\pi/g_c = 1$ μs (200 ns). Assuming $Q = 10^5$ at $B_0 = 0.5$ T in state-of-the-art superconducting cavities[72, 73] $g_c\kappa = 6.7$ (33) Rabi cycles can be obtained for $z_0 = 4.6$ nm (6.9 nm), where $\kappa = f/Q$ is the cavity loss rate.

Relaxation and Dephasing. We consider spin-lattice (phonon) relaxation and dephasing from a host of electrical noise sources, and compare them to gate times. Since silicon is not piezoelectric, spin-lattice relaxation occurs only via the deformation potential[74, 75]. For temperatures $T \ll \hbar\omega/k_B$, the spin relaxation time derived in the Supplemental Material[64] follows $T_1^{-1} = (\hbar\omega)^3(C_d/20\rho\pi\hbar^4)(|\lambda_{Zo}|/\Delta)^2$, where $|\lambda_{Zo}|/\Delta = \hbar\omega/4pE_z$ at the sweet spot, and $C_d = 4.9 \times 10^{-20}$ (eV)^2(s/m)^5. We obtain $T_1 = 20$ μs (5 μs) for $z_0 = 4.6$ nm (6.9 nm) at $B_0 = 0.5$ T that are 100 times longer *c.f.* bulk unstrained silicon at $B = 0.5$ T.[23, 57]

Random fluctuations in qubit splitting $\hbar\delta\omega(t)$ dephase the qubit. The dephasing rate from random telegraph signal (RTS) in charge trap occupation is $(T_2^*)^{-1} = (\delta\omega)^2\tau_S/2$, where $\delta\hbar\omega$ is qubit frequency shift, and τ_S is the average switching time.[36] We take $\tau_S = 10^3\tau_1$ as the worst case, since slower fluctuations can be suppressed by dynamical decoupling. Assuming a trap 50 nm away, we find $\delta E \sim 2,000$ V/m and a large window of $200,000$ V/m

(20,000 V/m) of gate space where $T_2^* > 2T_1$ at the sweet spot, for $z_0 = 4.6$ nm (6.9 nm). In comparison, the same analysis gives $T_2^* \sim 0.1$ ns for acceptor-based charge qubits with similar gate times. It is remarkable that in comparison, electrical noise has virtually no effect on coherence in our spin-orbit qubit, illustrating the advantages of inversion asymmetry and our spin-orbit qubit's sweet spot. We also find that dephasing from Johnson-limited gate voltage noise, and from two-level (tunneling) systems (TLS), are $\sim 10^7$ and $\sim 10^4$ times weaker, respectively, compared with RTS.[36] There are only a few spin resonance experiments on acceptors[58, 76–81], none of which feature strain and an interface.[50] We expect hyperfine-induced decoherence in $^{\mathrm{nat}}$Si to be weak since it has only 4.7 % of spin-bearing isotopes and hyperfine interactions are weaker for holes than electrons.[38] Meanwhile, ^{28}Si enrichment could be used to virtually eliminate the nuclear bath.[39]

The insensitivity to Johnson noise and tunneling TLS means spin-lattice T_1 limits coherence for few (or slow enough) traps at Si/SiO$_2$ interfaces. For $B = 0.5$ T, $r_1 > 10^4$ single qubit gates, $r_{2dd} > 10^3$ dipole-dipole two-qubit gates, and $r_{2c} \approx 25$ cavity-mediated two-qubit gates can be achieved in a T_1 limited coherence time. Therefore while T_1 is short compared to donors, many gate operations can performed. Since $T_1 \propto \omega^{-5}$, choosing $B = 0.25$ T increases all ratios favourably to $r_1 > 10^5$, $r_{2dd} \approx 10^4$, and $r_{2c} \approx 50$. Since T_1 is much longer at the $E_z = 0$ sweet spot, adiabatically sweeping to $E_z = 0$ opens a pathway for a long-lived quantum memory.

Conclusions. The proposed single-acceptor spin-orbit qubit exploits the tunability of the $J = 3/2$ manifold of acceptors and the associated quadrupolar SOC arising from the ion and interface potential, providing for (i) fast one-qubit and long-ranged two-qubit gates (ii) at a sweet spot where the qubit phase and all gate timings are insensitive to electrical fluctuations, (iii) avoiding entirely the need for exchange interactions, (iv) in an industrially relevant silicon platform. 10^5 single-qubit and 10^4 two-qubit gates could be possible in the qubit coherence time. Using cQED, dispersive single-spin readout, cavity-mediated spin-spin entanglement, and Jaynes-Cummings spin-photon entanglement are possible.

We thank R. Winkler, U. Zuelicke, M. Tong, and T. Kobayashi for helpful discussions. JS, JAM and SR acknowledge funding from the ARC Centre of Excellence for Quantum Computation and Communication Technology (CE110001027), and in part by the US Army Research Office (W911NF-08-1-0527). DC acknowledges funding through the ARC Discovery Project scheme.

[1] J. Majer, J. M. Chow, J. M. Gambetta, J. Koch, B. R. Johnson, J. A. Schreier, L. Frunzio, D. I. Schuster, A. A. Houck, A. Wallraff, A. Blais, M. H. Devoret, S. M. Girvin, and R. J. Schoelkopf, Nature **449**, 443 (2007).

[2] M. D. Shulman, O. E. Dial, S. P. Harvey, H. Bluhm, V. Umansky, and A. Yacoby, Science **336**, 202 (2012).

[3] R. Barends, J. Kelly, A. Megrant, A. Veitia, D. Sank, E. Jeffrey, T. C. White, J. Mutus, A. G. Fowler, B. Campbell, Y. Chen, Z. Chen, B. Chiaro, A. Dunsworth, C. Neill, P. O'Malley, P. Roushan, A. Vainsencher, J. Wenner, A. N. Korotkov, A. N. Cleland, and J. M. Martinis, Nature **508**, 500 (2014).

[4] G. Waldherr, Y. Wang, S. Zaiser, M. Jamali, T. Schulte-Herbrüggen, H. Abe, T. Ohshima, J. Isoya, J. F. Du, P. Neumann, and J. Wrachtrup, Nature **506**, 204 (2014).

[5] M. Veldhorst, C. H. Yang, J. C. C. Hwang, W. Huang, J. P. Dehollain, J. T. Muhonen, S. Simmons, A. Laucht, F. E. Hudson, K. M. Itoh, A. Morello, and A. S. Dzurak, Nature **526**, 410 (2015).

[6] D. Loss and D. P. DiVincenzo, Phys. Rev. A **57**, 120 (1998).

[7] B. E. Kane, Nature **393**, 133 (1998).

[8] J. R. Petta, A. C. Johnson, J. M. Taylor, E. A. Laird, A. Yacoby, M. D. Lukin, C. M. Marcus, M. P. Hanson, and A. C. Gossard, Science **309**, 2180 (2005).

[9] J. T. Muhonen, J. P. Dehollain, A. Laucht, F. E. Hudson, R. Kalra, T. Sekiguchi, K. M. Itoh, D. N. Jamieson, J. C. McCallum, A. S. Dzurak, and A. Morello, Nature Nanotech **9**, 986 (2014).

[10] M. Veldhorst, J. C. C. Hwang, C. H. Yang, A. W. Leenstra, B. de Ronde, J. P. Dehollain, J. T. Muhonen, F. E. Hudson, K. M. Itoh, A. Morello, and A. S. Dzurak, Nature Nanotech **9**, 981 (2014).

[11] X. Hu and S. Das Sarma, Phys. Rev. Lett. **96**, 100501 (2006).

[12] D. Culcer, X. Hu, and S. Das Sarma, Appl. Phys. Lett. **95**, 073102 (2009).

[13] O. E. Dial, M. D. Shulman, S. P. Harvey, H. Bluhm, V. Umansky, and A. Yacoby, Phys. Rev. Lett. **110**, 146804 (2013).

[14] A. G. Fowler, M. Mariantoni, J. M. Martinis, and A. N. Cleland, Phys. Rev. A **86**, 032324

(2012).
[15] V. N. Golovach, M. Borhani, and D. Loss, Phys. Rev. B **74**, 165319 (2006).
[16] C. Flindt, A. S. Sørensen, and K. Flensberg, Phys. Rev. Lett. **97**, 240501 (2006).
[17] M. Trif, V. N. Golovach, and D. Loss, Phys. Rev. B **75**, 085307 (2007).
[18] M. Trif, V. N. Golovach, and D. Loss, Phys. Rev. B **77**, 045434 (2008).
[19] D. V. Bulaev and D. Loss, Phys. Rev. Lett. **95**, 076805 (2005).
[20] D. V. Bulaev and D. Loss, Phys. Rev. Lett. **98**, 097202 (2007).
[21] A. Pályi, P. R. Struck, M. Rudner, K. Flensberg, and G. Burkard, Phys. Rev. Lett. **108**, 206811 (2012).
[22] C. Kloeffel, M. Trif, P. Stano, and D. Loss, Phys. Rev. B **88**, 241405 (2013).
[23] R. Ruskov and C. Tahan, Phys. Rev. B **88**, 064308 (2013).
[24] X. Hu, Y.-x. Liu, and F. Nori, Phys. Rev. B **86**, 035314 (2012).
[25] J. M. Taylor, V. Srinivasa, and J. Medford, Phys. Rev. Lett. **111**, 050502 (2013).
[26] A. Blais, R.-S. Huang, A. Wallraff, S. M. Girvin, and R. J. Schoelkopf, Phys. Rev. A **69**, 062320 (2004).
[27] A. Wallraff, D. I. Schuster, A. Blais, L. Frunzio, R. S. Huang, J. Majer, S. Kumar, S. M. Girvin, and R. J. Schoelkopf, Nature **431**, 162 (2004).
[28] K. D. Petersson, L. W. McFaul, M. D. Schroer, M. Jung, J. M. Taylor, A. A. Houck, and J. R. Petta, Nature **490**, 380 (2012).
[29] Z.-L. Xiang, S. Ashhab, J. You, and F. Nori, Rev. Mod. Phys. **85**, 623 (2013).
[30] J. J. Viennot, M. C. Dartiailh, A. Cottet, and T. Kontos, Science **349**, 408 (2015).
[31] T. Jochym-O'Connor and S. D. Bartlett, Phys. Rev. A **93**, 022323 (2016).
[32] K. C. Nowack, F. H. L. Koppens, Y. V. Nazarov, and L. M. K. Vandersypen, Science **318**, 1430 (2007).
[33] S. Nadj-Perge, S. M. Frolov, E. P. A. M. Bakkers, and L. P. Kouwenhoven, Nature **468**, 1084 (2010).
[34] J. Medford, J. Beil, J. M. Taylor, E. I. Rashba, H. Lu, A. C. Gossard, and C. M. Marcus, Phys. Rev. Lett. **111**, 050501 (2013).
[35] P. Huang and X. Hu, Phys. Rev. B **90**, 235315 (2014).
[36] A. Bermeister, D. Keith, and D. Culcer, Appl. Phys. Lett. **105**, 192102 (2014).
[37] B. Golding and M. I. Dykman, (2003), arXiv:cond-mat/0309147v1.

[38] E. A. Chekhovich, M. M. Glazov, A. B. Krysa, M. Hopkinson, P. Senellart, A. Lemaître, M. S. Skolnick, and A. I. Tartakovskii, Nature Physics **9**, 74 (2012).

[39] A. M. Tyryshkin, S. Tojo, J. J. L. Morton, H. Riemann, N. V. Abrosimov, P. Becker, H.-J. Pohl, T. Schenkel, M. L. W. Thewalt, K. M. Itoh, and S. A. Lyon, Nature Materials **11**, 143 (2011).

[40] J. van der Heijden, J. Salfi, J. A. Mol, J. Verduijn, G. C. Tettamanzi, A. R. Hamilton, N. Collaert, and S. Rogge, Nano Lett. **14**, 1492 (2014).

[41] R. Winkler, Phys. Rev. B **70**, 125301 (2004).

[42] D. Culcer, C. Lechner, and R. Winkler, Phys. Rev. Lett. **97**, 106601 (2006).

[43] D. Culcer and R. Winkler, Phys. Rev. B **76**, 195204 (2007).

[44] R. Winkler, D. Culcer, S. J. Padadakis, B. Habib, and M. Shayegan, Semicond. Sci. Tech. **23**, 114017 (2008).

[45] J. Luttinger and W. Kohn, Phys. Rev. **97**, 869 (1955).

[46] F. A. Zwanenburg, C. E. W. M. van Rijmenam, Y. Fang, C. M. Lieber, and L. P. Kouwenhoven, Nano Lett. **9**, 1071 (2009).

[47] Y. Hu, F. Kuemmeth, C. M. Lieber, and C. M. Marcus, Nature Nanotech **7**, 47 (2011).

[48] V. S. Pribiag, S. Nadj-Perge, S. M. Frolov, J. W. G. van den Berg, I. van Weperen, S. R. Plissard, E. P. A. M. Bakkers, and L. P. Kouwenhoven, Nature Nanotech **8**, 170 (2013).

[49] B. Voisin, R. Maurand, S. Barraud, M. Vinet, X. Jehl, M. Sanquer, J. Renard, and S. De Franceschi, Nano Lett. **16**, 88 (2016).

[50] J. A. Mol, J. Salfi, R. Rahman, Y. Hsueh, J. A. Miwa, G. Klimeck, M. Y. Simmons, and S. Rogge, Appl. Phys. Lett. **106**, 203110 (2015).

[51] J. Salfi, J. A. Mol, R. Rahman, G. Klimeck, M. Y. Simmons, L. C. L. Hollenberg, and S. Rogge, Nature Commun. **7**, 11342 (2016).

[52] A. Morello, J. J. Pla, F. A. Zwanenburg, K. W. Chan, K. Y. Tan, H. Huebl, M. Möttönen, C. D. Nugroho, C. Yang, J. A. van Donkelaar, A. D. C. Alves, D. N. Jamieson, C. C. Escott, L. C. L. Hollenberg, R. G. Clark, and A. S. Dzurak, Nature **467**, 687 (2010).

[53] M. Fuechsle, J. A. Miwa, S. Mahapatra, H. Ryu, S. Lee, O. Warschkow, L. C. L. Hollenberg, G. Klimeck, and M. Y. Simmons, Nature Nanotech **7**, 242 (2012).

[54] J. A. Miwa, J. A. Mol, J. Salfi, S. Rogge, and M. Y. Simmons, Appl. Phys. Lett. **103**, 043106 (2013).

[55] G. L. Bir, E. I. Butekov, and G. E. Pikus, J. Phys. Chem. Solids **24**, 1467 (1963).

[56] S. G. Pavlov, N. Deßmann, V. N. Shastin, R. K. Zhukavin, B. Redlich, A. F. G. van der Meer, M. Mittendorff, S. Winnerl, N. V. Abrosimov, H. Riemann, and H. W. Hübers, Phys. Rev. X **4**, 021009 (2014).

[57] G. L. Bir, E. I. Butikov, and G. E. Pikus, J. Phys. Chem. Solids **24**, 1475 (1963).

[58] A. Köpf and K. Lassmann, Phys. Rev. Lett. **69**, 1580 (1992).

[59] J. Schrieffer and P. Wolff, Phys. Rev. **149**, 491 (1966).

[60] R. Winkler, Spin-Orbit Coupling Effects in Two-Dimensional Electron and Hole Systems, Springer Tracts in Modern Physics, Vol. 191 (Springer Berlin Heidelberg, Berlin, Heidelberg, 2003).

[61] A. Baldereschi and N. Lipari, Phys. Rev. B **8**, 2697 (1973).

[62] P. Lawaetz, Phys. Rev. B **4**, 3460 (1971).

[63] J. Bernholc and S. Pantelides, Phys. Rev. B **15**, 4935 (1977).

[64] See the Supplemental Material which gives details on interactions with magnetic fields and strain, acceptor states in the spherical spin-3/2 basis, an analytic model for low energy states, details on Schrieffer-Wolff transformations for EDSR, spin-dependent dipole-dipole interactions, spin-lattice relaxation, describes dephasing from electric field noise, and gives details on the numerical Kohn-Luttinger calculations.

[65] G. K. Celler and S. Cristoloveanu, Journal of Applied Physics **93**, 4955 (2003).

[66] C. C. Lo, M. Urdampilleta, P. Ross, M. F. Gonzalez-Zalba, J. Mansir, S. A. Lyon, M. L. W. Thewalt, and J. J. L. Morton, Nature Publishing Group **14**, 490 (2015).

[67] G. D. J. Smit, S. Rogge, J. Caro, and T. M. Klapwijk, Phys. Rev. B **70**, 035206 (2004).

[68] J. J. Pla, K. Y. Tan, J. P. Dehollain, W. H. Lim, J. J. L. Morton, D. N. Jamieson, A. S. Dzurak, and A. Morello, Nature **489**, 541 (2012).

[69] K. D. Petersson, C. G. Smith, D. Anderson, P. Atkinson, G. A. C. Jones, and D. A. Ritchie, Nano Lett. **10**, 2789 (2010).

[70] J. Salfi, J. A. Mol, R. Rahman, G. Klimeck, M. Y. Simmons, L. C. L. Hollenberg, and S. Rogge, Nature Materials **13**, 605 (2014).

[71] B. Koiller, X. Hu, and S. Das Sarma, Phys. Rev. Lett. **88**, 027903 (2001).

[72] N. Samkharadze, A. Bruno, P. Scarlino, G. Zheng, D. P. DiVincenzo, L. DiCarlo, and L. M. K. Vandersypen, Phys. Rev. Applied **5**, 044004 (2016).

[73] S. E. d. Graaf, A. V. Danilov, A. Adamyan, T. Bauch, and S. E. Kubatkin, Journal of Applied Physics **112**, 123905 (2012).

[74] H. Ehrenreich and A. W. Overhauser, Phys. Rev. **104**, 331 (1956).

[75] G. P. Srivastava, Physics of Phonons (Adam Hilger, New York, 1990).

[76] J. Hensel and G. Feher, Phys. Rev. **129**, 1041 (1963).

[77] H. Neubrand, Phys. Status Solidi (b) **86**, 269 (1978).

[78] H. Neubrand, Phys. Status Solidi (b) **90**, 301 (1978).

[79] H. Tezuka, A. R. Stegner, A. M. Tyryshkin, S. Shankar, M. L. W. Thewalt, S. A. Lyon, K. M. Itoh, and M. S. Brandt, Phys. Rev. B **81**, 161203 (2010).

[80] A. R. Stegner, H. Tezuka, T. Andlauer, M. Stutzmann, M. L. W. Thewalt, M. S. Brandt, and K. M. Itoh, Phys. Rev. B **82**, 115213 (2010).

[81] Y. P. Song and B. Golding, Europhysics Letters **95**, 47004 (2011).